

AUTOMATED GROUND CONTROL POINT ACQUISITION FOR GEOMETRIC
CORRECTION OF SPACEBORNE SAR DATA

Hiromichi Maruyama
National Institute Of Resources, STA
1-11-39 Nagata-cho, Chiyoda-ku, Tokyo, 100
Japan
Commission I

1. Introduction

Geometric correction of SAR data is required in order to do multi-temporal and multi-sensor analysis. In the past, geometric correction has been performed using parameters describing the platform motion, GCPs (Ground Control Points) and a DTM (Digital Terrain Model) if a mountainous area data was being imaged ([1]). In mountainous areas, however, it is very difficult to identify control points on SAR imagery, because there are generally few man-made features and imagery can exhibit extreme local distortions due to topography. To solve these difficulties, use of simulated SAR image generated with the aid of DTM, a simple radar scattering model and a knowledge of the SAR sensing geometry has been investigated.

The high level of similarity found between simulated and real SEASAT images indicates that simulated image chips could be utilized to automatic GCP acquisition. Since DTMs are in general sampled on a regular geographic grid, the chips themselves would also provide the geodetic information needed for SAR image rectification.

Figure 1 shows a portion of a SEASAT scene of a mountainous region near Anderson River, British Columbia in Canada which is used as the test area in the following. From next section of this paper, generation of simulated SAR image, image matching results and a proposed geometric correction procedure with automated control point acquisition are described.

2. Generation of simulated SAR image

To simplify the calculation, the radar look angle and the spacecraft heading are assumed to be constant. Backscatter from unit area on the terrain surface is assumed to be the cosine of the incidence angle with respect to surface normal.

On these assumptions, a simulated SAR image is generated from a DTM only once we specify RANGE/AZIMUTH pixel size, look angle and spacecraft heading. The simulated image generation process is as follows.

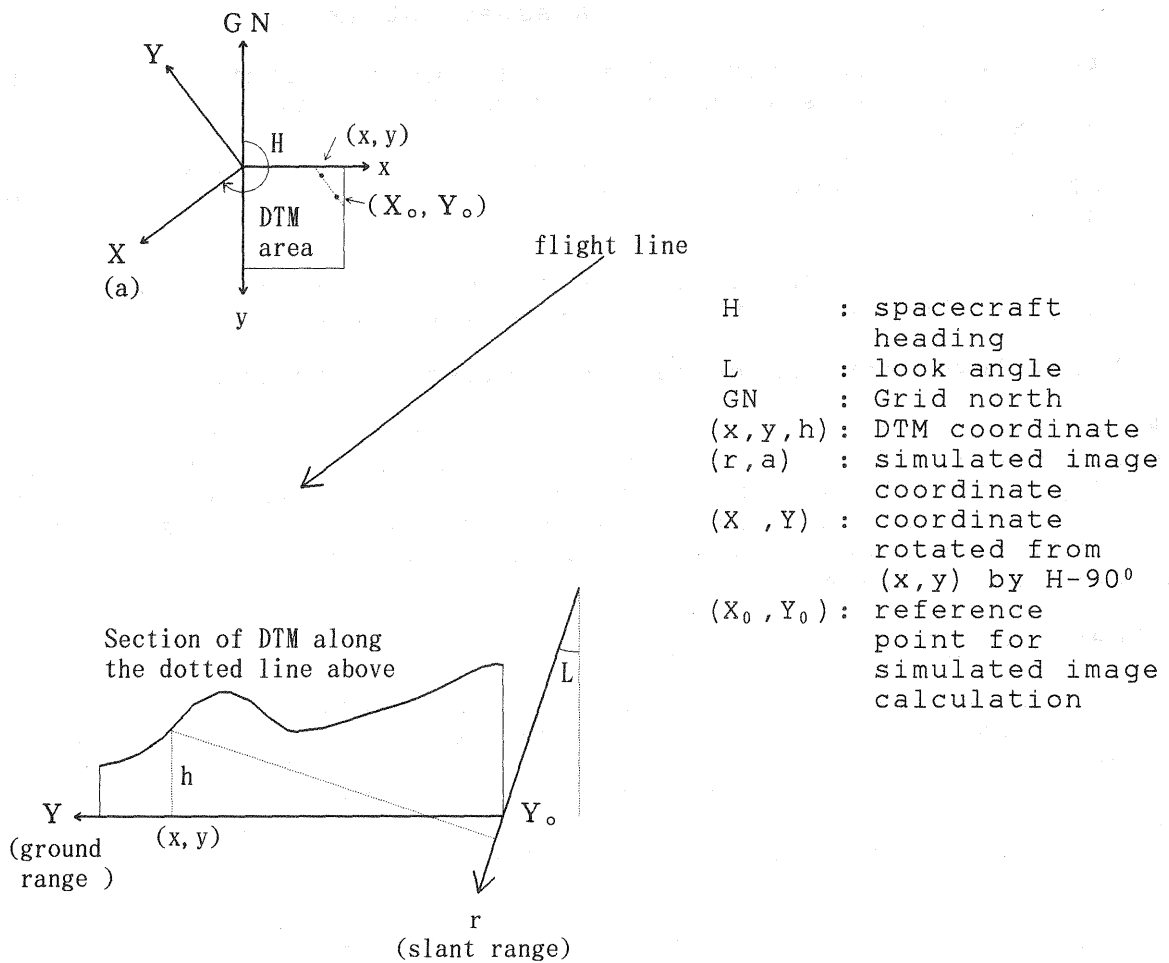
- (1) Get the transformation 'f' from the DTM coordinates (x,y,h) to the simulated image coordinates (r,a). Figure 2 shows the relation between two coordinates.

$$\begin{aligned} X &= \sin H \cdot x - \cos H \cdot y \\ Y &= \cos H \cdot x + \sin H \cdot y \end{aligned}$$

Figure 1 A portion of a SEASAT scene



Figure 2 DTM coordinate and the simulated image coordinate



$$r = (Y - Y_0) \cdot \sin L - h \cdot \cos L \text{ (slant range representaiton)}$$

$$a = X - X_0$$

$$r = (Y - Y_0) - h \cdot \cot L \text{ (ground range representaiton)}$$

$$a = X - X_0$$

- (2) Calculate the size of the simulated image from the boundary coordinates, the highest and lowest elevations in the DTM given.
- (3) Based on the specified RANGE/AZIMUTH pixel size, set the grid on the image frame got in (2).
- (4) For each grid point (mr,ma) in (3), get the inverse image by 'f' which is not included in the radar shadow area. The inverse image is on a line in the DTM coordinates system and consist of discrete points or intervals.
- (5) For each discrete point (x,y,h) which is included in the invese image of (mr,ma), calculate the incidence angle of RADAR with respect to the surface normal. Here, the incidence angle i is expressed as

$$\cos i = \cos L \cdot \cos S + \sin L \cdot \sin S \cdot \cos(H-A)$$

S:slope
A:aspect at (x,y)

As (x,y) is not always a grid point, bilinear interpolation is used for getting hight, slope and aspect at (x,y).

At each interval I which is included in the inverse image of (mr,ma), radar look direction is perpendicular to the DTM surface.

- (6) Grey level at (mr,ma) is the sum of cosine of incidence angles and the length of intervals calculated in (5).
- (7) Grey level conversion can be applied if required.

Figure 3 shows the simulated SAR image generated by the method mentioned above and the area is corresponding to that of Figure 1. This simulation utilized a 16km x 16km DTM derived from digitization of elevation contours on available 1:50,000 topographic map. The characteristics of the image is summerized in Table 1.

3. Image matching

For SEASAT image and its simulated image, image matching experiments were performed using the same method described in reference [3]. First, 18 CPs(control points) were acquired manually to define an accurate affine transformation between the SAR and the simulated image. (This transformation will be referred to as the seed transformation.)

Next, 30 image chips (which will be referred to as RCPs) were extracted from the reference image (The SEASAT image was used as a reference image here). The RCP, each of size 64 pixels by

Figure 3 The simulated SEASAT image

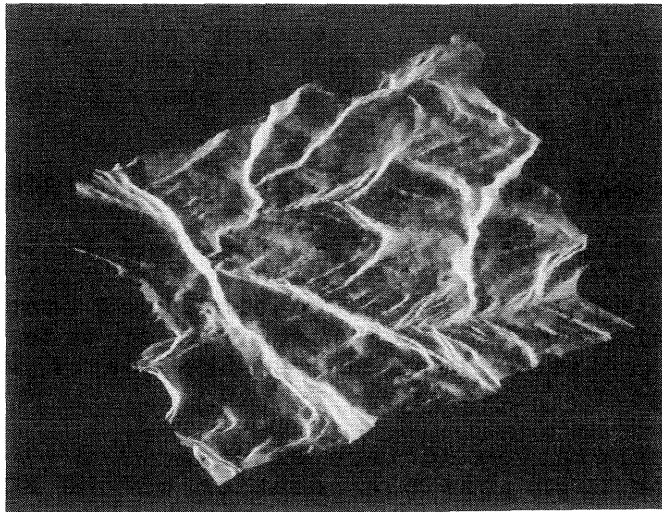
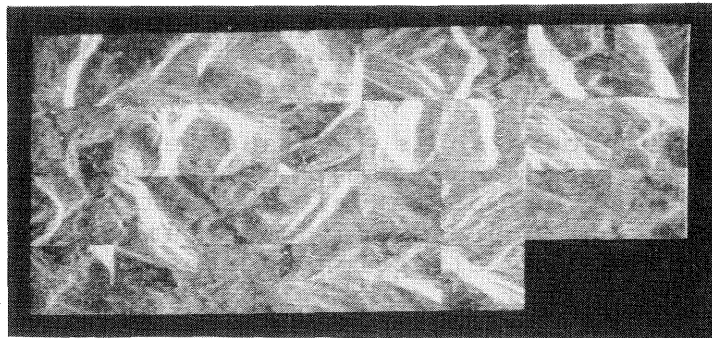


Table 1 Characteristics of simulated image

pixel size (ground range)	25 m
(azimuth)	25 m
look angle	23 °
heading (from UTM Grid north)	208.35 °
grey-level compression	square root of power

Figure 4 The 30 RCPs (size 64 pixels and 64 lines) utilized in the matching experiments



64 lines, are shown in Figure 4.

Finally, 12 matching experiments were performed in order to check the effects of RCP size and the noise reduction filtering of SEASAT image. The filtering included null filtering and adaptive filtering with speckle-reducing filter proposed by Frost et al [4].

The following steps were taken for each of 30 RCPs.

- (1) Select a RCP which has specified size and filtering option.
- (2) Extract a search window from the simulated image of size $(M+16) \times (M+16)$ where the RCP itself is of size $M \times M$. Use the seed transformation to set the search window on the reference image.
- (3) Generate a correlation surface of size 17×17 by computing, for each possible location of the RCP within the search window, the average correlation between the RCP and the corresponding subwindow pixels.
- (4) Search the correlation surface for the peak value. Refine the estimate of the best match location by fitting a 3×3 area, centred on the peak correlation location, with a two dimensional biquadratic polynomial and interpolate the functional peak to subpixel accuracy.

After application of the matching procedure, the seed CPs were deleted and the affine transformation was redefined based on the RCPs only. A RMS position error of these RCPs was calculated and used as one measure of the accuracy of the automated CP acquisition process.

Table 2 shows the summary of matching results. From the summary of results, we can see that

- (1) Adaptive filtering is an effective procedure to increase correlation coefficient and hence real and simulated image similarity.
- (2) The larger the window size is, the smaller RMS error is. In addition, RMS error in the case of the window size 48×48 is almost same as that of manual acquisition of 18 CPs in the pixel direction (corresponding to range direction) and better than in the line direction (corresponding to azimuth direction).
- (3) Adaptive filtering improve RMS error, but not significantly.

4. Stable RCP

There is a tendency that the larger RCP size, the smaller RMS error is. Calculation time, however, increase in proportion to square of the RCP size. Therefore if some method to find smaller RCP which promises accurate matching will be very preferable. Such RCPs are expected to attain almost the same

Table 2 Summary of matching results

RCP size	filter option*	RMS error of RCPs		Number of failures	Median correlation coefficient
		pixel (range)	line (azimuth)		
16	NFL	3.0 pixel	2.4 pixel	3	0.60
x	7x7	2.7	2.4	3	0.66
16	11x11	2.7	3.0	4	0.67
32	NFL	2.5	1.8	2	0.61
x	7x7	2.2	1.8	2	0.68
32	11x11	2.1	1.7	2	0.70
48	NFL	1.7	1.2	1	0.64
x	7x7	1.6	1.1	1	0.71
48	11x11	1.6	1.1	1	0.72
64	NFL	1.8	1.0	3	0.64
x	7x7	1.5	0.9	1	0.72
64	11x11	1.5	0.9	1	0.72
manual acquisition		1.6	1.6		

*

NFL = no prefiltering

7x7 = adaptive filtering 7x7 window

11x11= adaptive filtering 11x11 window

best match coordinate irrespective of RCP size, that is stable in RCP size change.

Here, instability of i-th RCP was defined as

$$INS_i = \sqrt{\sum_{(P,L) \in B_i} [(P-P_0)^2 + (L-L_0)^2] / (\#B_i - 1)}$$

where

B_i :subset of $A_i = \{(P,L) \mid \text{the best match location of } i\text{-th RCP chip of the size } 64 \times 64, 48 \times 48 \text{ and } 32 \times 32\}$

$\#B_i$:number of elements of the set B

(P_0, L_0) :the best match location in case of RCP size 64×64 with 11×11 adaptive filter

Two different sets, B_i^1 and B_i^2 , were chosen as B_i . Their definitions were as follows.

$$B_i^1 = \{(P,L) \in A_i \mid \text{RCP size is } 64 \times 64, 48 \times 48 \text{ or } 32 \times 32\}$$

$$B_i^2 = \{(P,L) \in A_i \mid \text{RCP size is } 64 \times 64 \text{ or } 48 \times 48\}$$

The RCP chip which has the instability less than 1.0 pixel was regarded as the stable chip and RMS error was calculated using stable chips only. The results are as Table 3. RCP size was assumed 32×32 if set B_i^1 's were used, 48×48 if B_i^2 's were used.

Table 3 RMS error of stable RCPs

RCP size	filter option	pixel (range)	line (azimuth)	Number of Stable RCPs
32	NFL	1.3	1.1	16
x	7x7	1.2	1.0	
32	11x11	1.2	1.0	
48	NFL	1.5	0.9	22
x	7x7	1.6	0.9	
48	11x11	1.6	0.9	

Table 3 indicates that, when the RCP size is 48x48, RMS error of stable RCPs only is almost same as that of all RCPs. On the other hand, when the RCP size is 32x32, RMS is improved significantly by excluding unstable RCPs. Therefore the characterization of stable RCPs seems very important to attain good matching and save computaion time.

Table 3 also indicates adaptive filtering is not effective for reducing RMS error for stable RCPs. Therefore, we hereafter consider only the matching without prefiltering.

Figure 5 shows the distributions of RCPs as a function of peak correlation coefficient. Those RCPs which are not stable are indicated by hatched areas. Figure 5 indicates stable RCPs are not necessarily characterized by high peak correlations. However, a RCP which has high peak correlation has high possibility to be stable. Therefore if we can predict the peak correlation coefficient of a RCP, only stable RCP candidates can be chosen before matching procedure.

Expected correlation coefficient E, defined as follows, can be used to predict peak correlation coefficient.

$$E = \frac{1}{\sqrt{(5/4 + 1/4 * m_R^2 / \sigma_R^2)}}$$

R:RCP chip

The simulated image can be overlaid on SAR image (reference image) using the seed transformation.

m_R : mean value of the portion of overlaid image equivalent to RCP R

σ_R : standard deviation of the image mentioned above

Figure 6 shows the relation between the expected correlation and the peak correlation. The relation itself exhibits a correlation level of 0.91 if RCP size is 32x32 and 0.88 if RCP size is 48x48.

Figure 5 Distributions of peak correlation for RCPs of sizes 32x32 and 48x48 (with NFL)

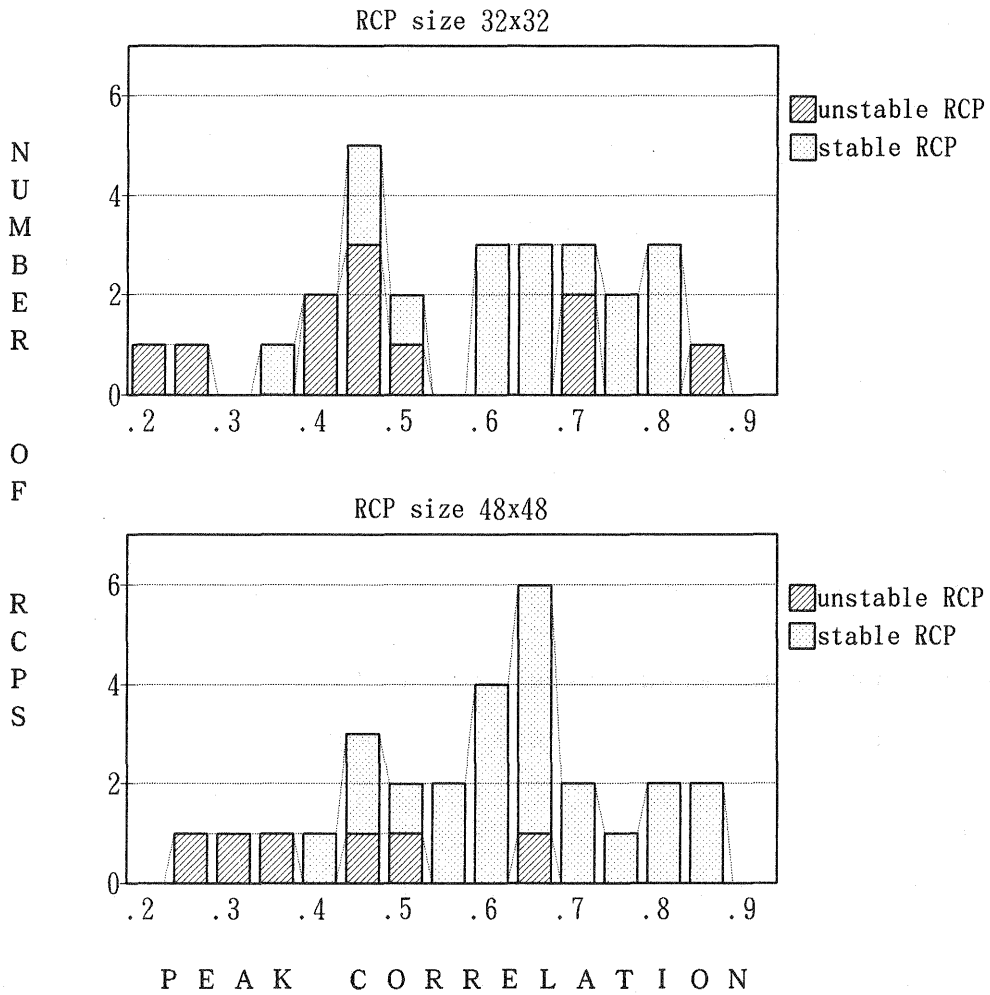
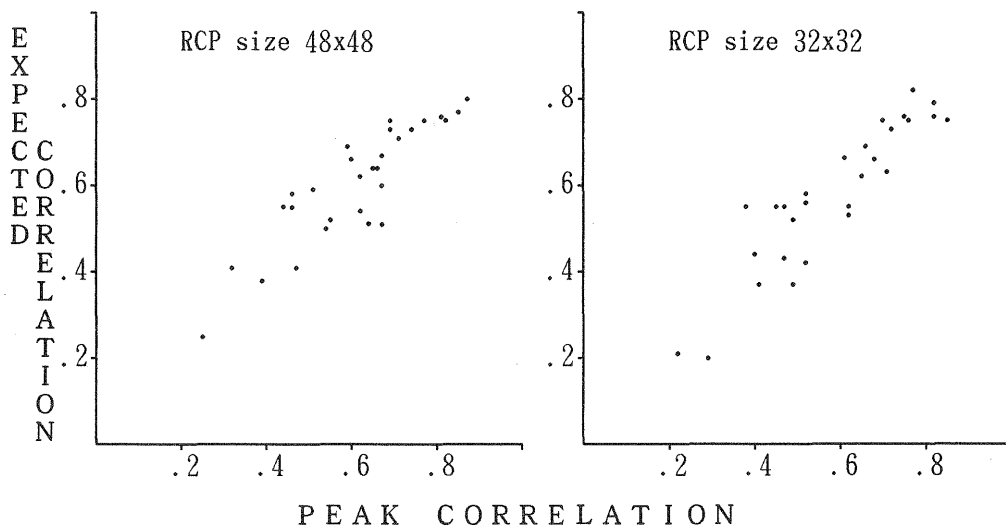


Figure 6 Distributions of expected correlation vs peak correlation (with NFL)



5. Automated CP acquisition

In section 3, 18 CPs were acquired manually before the matching experiment in order to get accurate transformation between the real SAR image and its simulated image, and to check the similarity between them. However, automatic control point acquisition has no meaning if many seed CPs are required. Therefore another experiment was performed using only 4 seed CPs and 30 RCPs.

The results of these experiments shows same tendency when 18 seed CPs were used. That is, if the RCP size is 48x48, an accurate transformation in terms of RMS error can be obtained without special considerations. On the other hand, only stable RCPs should be accepted when RCP size is 32x32. In both cases, adaptive filtering does not improve RMS error.

Based on the results acquired so far, the following method for geometric correction of spaceborne SAR image in mountainous area can be proposed.

- (1) Get approximate orbit parameters of spacecraft which are accurate enough to get the simulated image similar to SAR image.
 - (2) Generate the simulated image from DTM.
 - (3) Select the locations where CPs are required.
 - (4) Corresponding to these locations, find the stable RCP candidates based on the expected correlation.
 - (5) Select seed CPs and perform matching.
 - (6) Define an affine or quadratic transformations from simulated image to SAR image based on automatically acquired CPs and rejects CPs which has big RMS errors.
 - (7) Recompute transformations using only the remaining RCPs. Go back to (3), if number of CPs is not enough or positional distribution of RCPs is not appropriate.
 - (8) Using the transformation defined in (7) and DTM, get geometrically corrected SAR image.
- or
- (8') Estimate the geodetic coordinates of the stable RCP centres and use these to define physical transformation from the raw image to the geographic coordinates.

To make this flow practical, it is necessary to characterize stable RCPs more clearly and to prepare accurate DTMs. However, if these conditions are satisfied, geometric correction of SAR data in mountainous area seems to be attainable with small manual work and time as RCP candidates can be determined from orbit parameters before the image is acquired.

6. Conclusions

- simulated SAR image derived only DTM can be used for automated CP acquisition for SAR data in mountainous area.
- rough flow of was presented for geometric correction of spaceborne SAR data in mountainous area.
- characterization of stable RCPs is required to make the automated CP acquisition more practical.
- expected correlation seems effective for pre-screening of unstable RCPs.

7. Acknowledgement

This work was done while I stayed at CCRS with the support of Science and Technology Agency of JAPAN. The author wish to thank Dr. B. Guindon for providing the SEASAT data and many advices.

8. References

- [1] Guindon, B., Goodenough, D.G. and Teillet, P.M.-- The Role of Digital Terrain Models in the remote sensing of forests, Canadian Journal of Remote Sensing Vol.8, pp4-16, 1982.
- [2] Naraghi, M., Stromberg, W. and Daily, M.-- Geometric Rectification of Radar Imagery Using Digital Elevation Model, Photogrammetric Engineering and Remote Sensing Vol.49, pp195-199, 1983.
- [3] Guindon, B.-- Automated Control Point Acquisition in Radar-Optical Image Registration, Canadian Journal of Remote Sensing Vol.11, pp103-112, 1985.
- [4] Frost, V.S., Stiles, J.A., Shanmugan, K.S. and Holtzmann, J.C.--A Model for Radar Images and Its Applications to Adaptive Digital Filtering of Mutiplicative Noise, IEEE Transactions on Pattern Analysis and Machine Intelligence, PAMI-4, pp157-166, 1982.
- [5] Guindon, B. and Maruyama, H.-- Automated Matching of Real and Simulated SAR Imagery as a Tool for Ground Control Point Acquisition, Canadian Journal of Remote Sensing Vol.12, pp149-158, 1986.

